Double-exchange model for noninteracting electron spins coupled to a lattice of classical spins: Phase diagram at zero temperature

David Pekker,[1] Swagatam Mukhopadhyay,[1] Nandini Trivedi,[2] and Paul M. Goldbart[1]
[1]*Department of Physics, University of Illinois, 1110 West Green Street, Urbana, Illinois 61801-3080, USA*
[2]*Department of Physics, The Ohio State University, 191 West Woodruff Avenue, Columbus, Ohio 43210, USA*
(Received 25 February 2005; revised manuscript received 23 May 2005; published 11 August 2005)

The analytical zero-temperature phase diagram of the double exchange model for classical background spins as a function of the carrier density and Hund's coupling in the entire range of these parameters is presented. By constructing a continuum field theory we explore the possibility of a continuous phase transition from ferromagnetic state to a gently varying textured state. We find such a transition in and below two dimensions and show that the emerging stable state is a spin-spiral which survives the tendency towards phase separation into commonly considered phases, and is also energetically favored to the canted state, for low carrier density.

DOI: 10.1103/PhysRevB.72.075118 PACS number(s): 75.30.Et, 75.47.Lx

I. INTRODUCTION

The double-exchange model (DEM) describes the motion of noninteracting itinerant electrons through a lattice of classical spins to which the electron spins are coupled. This model is relevant, e.g., to the manganites, which show colossal magnetoresistance. Although electron-phonon interactions play an important role in the manganites through a Jahn-Teller effect,[1] some of the key features of the strongly coupled spin, charge, and lattice degrees of freedom are captured by a DEM with lattice-distortion effects. Another class of materials for which the DEM is relevant are the dilute magnetic semiconductors, such a GaAs doped with Mn, which are important for spintronics applications.[2] In these materials, the $S=5/2$ local moments on the Mn sites are exchange coupled to the hole carriers generated by substituting Mn for Ga. While a more realistic model would include the effects of disorder[3,4] arising from the random substitution of the Mn atoms, as well as spin-orbit coupling effects,[5,6] a careful study of the DEM is a necessary first step.

Thus, the DEM is a paradigm for a wide class of materials that show a strong coupling between the charge and spin degrees of freedom. Pioneering work on this model focused on the ferromagnetic and canted antiferromagnetic phases at nonzero temperature.[7] Over the past few years, the DEM has received renewed attention, stimulated in part by the numerical studies reported in Refs. 8 and 9, where the zero-temperature phase diagram of the simple DEM has been explored. More elaborate extensions of the DEM—intended to move it closer to real systems by augmenting it with physical processes such as the super-exchange and Coulomb interactions, disorder, and Jahn-Teller distortions, etc.—have also been investigated over the past few years. For example, the stability of a spin spiral state in one extension of the model was examined in Ref. 10 and was contrasted with the stability of the canted state. The ground state of a model augmented with Coulomb interactions and large Hund coupling was addressed in Ref. 11. The instability of the homogeneous canted state with respect to phase separation, for large Hund coupling in a model that includes tunable super-exchange interaction, was studied in Ref. 12. The phase diagram of a three-dimensional model in the infinitely large Hund-coupling limit was studied in Ref. 13, and near the Curie temperature an instability with respect to spontaneous translational symmetry breaking was proposed, as was the possibility of phase separation. Recently, Ref. 14 addressed the stability of the spin spiral state as the ground state of the DEM in the large-S limit.

In spite of the considerable amount of theoretical and numerical work on the DEM, the continuous phase transition from the ferromagnetic phase to a spin-textured phase remains incompletely understood. Considerable attention has been paid to the model in the infinite Hund-coupling regime, motivated by the fact that in the manganites, the Hund coupling is large, compared with the electronic bandwidth. The zero-temperature phase diagram has been recently studied in Ref. 15 within dynamical mean field theory (DMFT) for the entire range of carrier concentrations and Hund coupling. It was shown that the stable ground state in different regions of parameter space is either a ferromagnet, or a commensurate antiferromagnet, or some incommensurate phase with an intermediate wave vector. Moreover, a second-order phase transition (from the ferromagnetic to the incommensurate phase) and a first-order transition (from the antiferromagnetic phase to a region of phase separation) were identified.

In this paper, we address the magnetic ordering of the single-band DEM with classical background spins at zero temperature (ignoring orbital or charge ordering). In contrast to previous work, which involved either a numerical approach[8] or the DMFA,[15,16] we use a continuum field theory and a gradient expansion to determine the critical line of continuous phase transitions separating the ferromagnetic and textured phases in the parameter space of electron density and Hund coupling. This approach allows us to consider all possible *long wavelength textures* that can emerge from the DEM. We argue that the spin spiral is the energetically favored one from amongst this class of textures. As is well known, the ground state of the DEM is phase separated at large values of the Hund coupling. However, by explicitly comparing the energetics of phase separation for commonly considered textures, we argue that there is a region of phase space in which the continuous transition survives the ten-

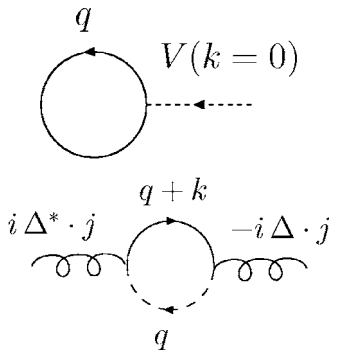

FIG. 1. Lowest-order Feynman diagrams (1 and 2): solid lines represent aligned electron propagators, dashed lines represent anti-aligned electron propagators, curly lines represent Δ_α, and dotted lines represent $\partial_\alpha \hat{\mathbf{n}} \cdot \partial_\alpha \hat{\mathbf{n}}$.

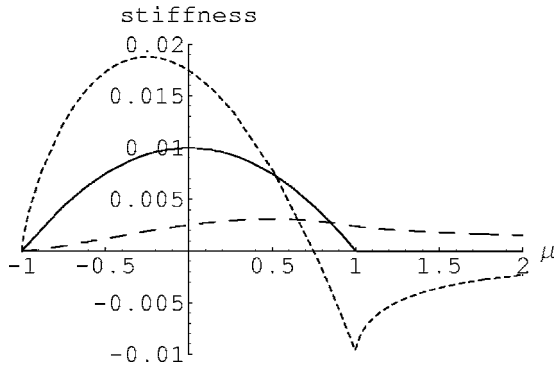

FIG. 2. Ferromagnetic stiffness in dimension d for $d=1.5$ (dotted), $d=2$ (solid), and $d=3$ (dashed). Here, $J_H=1$ and $J_{AF}=0$. Note that for $d=2$, the stiffness becomes zero at $\mu=J_H$ but does not become negative.

dency towards phase separation. We also show that the spin spiral state is favored, energetically, over the canted state, thereby making precise the nature of the emergent "incommensurate state" found in earlier works.[8,15,16] We present the phase diagram of the model, after including the commonly considered candidate phases for a preemptive phase separation at high Hund coupling. Our phase diagram looks qualitativly identical to the numerical and DMFA diagrams.[8,15,16] The one-dimensional DEM with quantum background spins ($S=1/2$) was analyzed via DMRG, and was also found to have a similar, but somewhat more complicated, phase diagram, which also includes a spin spiral phase.[17] In systems for which the Hund coupling is small (e.g., the cobaltates, diluted magnetic semiconductors, etc.) and the disorder is low, the approach used here may be of relevance.

The present paper is organized as follows. In Sec. II a continuum version of the DEM is derived. The symmetries of this continuum version are considered and the electronic degrees of freedom are integrated out, yielding an effective Hamiltonian for the background spins within a gradient expansion. A line of continuous phase transitions is determined, and it is shown that the spin-spiral state is the emergent stable state. In Sec. III the issue of whether the phase transition from the ferromagnetic states to the spin spiral state is preempted by another transition (to either an antiferro/ferrmagnetic microphase-separated state or to a canted ferromagnetic state) is considered. It is shown that there is a region of the phase diagram in which the spin spiral state is a stable state.

II. DOUBLE-EXCHANGE MODEL; ANALYTICAL STRATEGY

The double-exchange model describes noninteracting itinerant electrons moving on a lattice of static "background" spins whose moments are typically large compared to that of the electron spins, and hence may be treated classically. The Hamiltonian is taken to be

$$H = -t \sum_{\langle i,j\rangle a} (c_{ia}^\dagger c_{ja} + \text{h.c.}) - \frac{J_H}{S} \sum_{jab} \mathbf{S}_j \cdot c_{ja}^\dagger \boldsymbol{\sigma}_{ab} c_{jb} + \frac{J_{AF}}{S^2} \sum_{\langle i,j\rangle} \mathbf{S}_i \cdot \mathbf{S}_j, \tag{2.1}$$

where the first, second, and third terms respectively describe electronic hopping, double-exchange, and super-exchange couplings. Here, $\mathbf{S}_i$ is the background spin at lattice site i, which we approximate as a classical vector, J_H/S is the strength of the ferromagnetic Hund coupling, and J_{AF}/S^2 is the strength of the antiferromagnetic coupling between the localized spins. Aspects of the microscopic origin of this Hamiltonian are discussed, e.g., in Refs. 5, 18, and 19. We shall explore the J_H vs. electron density phase-diagram, considering J_{AF} to be vanishingly small. However, for technical reasons to be explained later, we shall need J_{AF} to be nonzero. Earlier work has mostly focused on the J_{AF} vs. electron density phase diagram of the model in the regime in which J_H is very large, so that the electrons are aligned with the background spins.

It is convenient to transform to a new spin basis at each lattice site, so that the local part of the Hamiltonian (i.e., the part that dominates at large J_H) is diagonal. To this end, we rewrite Eq. (2.1) in terms of the new operators $\{d_i^\dagger, d_i\}$ and $\{e_i^\dagger, e_i\}$ which are, respectively, the creation and annihilation operators associated with the spin basis aligned and anti-aligned with the background spin direction at site j:

$$\begin{pmatrix} c_{\uparrow j} \\ c_{\downarrow j} \end{pmatrix} = (\gamma_j \ \gamma_j^\perp) \begin{pmatrix} d_j \\ e_j \end{pmatrix}, \tag{2.2}$$

where the spinors γ_j and $\gamma_j^\perp$ are defined in terms of the the polar and azimuthal angles of the background spin direction at site j, i.e., θ_i and ϕ_i, and are given by

$$\gamma_j = e^{+i\chi_j} \begin{pmatrix} e^{-i\phi_j/2} \cos\dfrac{\theta_j}{2} \\ e^{+i\phi_j/2} \sin\dfrac{\theta_j}{2} \end{pmatrix}, \tag{2.3a}$$

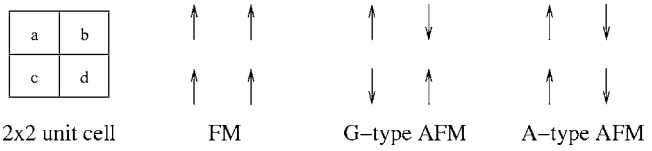

FIG. 3. Arrangements of background spins on the 2×2 plaquettes that are considered in the text.

$$\gamma_j^{\perp} = e^{-i\chi_j}\begin{pmatrix} -e^{-i\phi_j/2}\sin\dfrac{\theta_j}{2} \\ e^{+i\phi_j/2}\cos\dfrac{\theta_j}{2} \end{pmatrix}. \tag{2.3b}$$

γ and $\gamma_\perp$ form an orthonormal local basis corresponding to the aligned and antialigned spin states. This mapping is defined up to a phase factor χ_j, which is a gauge freedom.[21] Note that in the aligned antialigned spin basis, the Hund's term is diagonal. The kinetic energy term in this basis is

$$-t\sum_{\langle i,j\rangle}(d_i^{\dagger}\gamma_i^{*}\cdot\gamma_j d_j + e_i^{\dagger}\gamma_i^{\perp *}\cdot\gamma_j^{\perp}e_j + d_i^{\dagger}\gamma_i^{*}\cdot\gamma_j^{\perp}e_j + e_i^{\dagger}\gamma_i^{\perp *}\cdot\gamma_j d_j + \text{h.c.}). \tag{2.4}$$

We derive the continuum limit of the Hamiltonian,[23] defined on a hypercubic lattice, by expanding the kinetic energy term up to second order in gradients of the angles θ, ϕ, and χ and the electronic operators d and e. In the continuum limit, the Hamiltonian is (up to the corresponding gauge transformation) given by

$$H = -\int d\mathbf{x}\Bigg[\psi^{\dagger}(\mathbf{x})\left((\partial_\alpha - iA_\alpha)^2 + \frac{1}{4}(\partial_\beta\hat{\mathbf{n}}\cdot\partial_\beta\hat{\mathbf{n}}) - J_{\mathrm{H}}\right)\psi(\mathbf{x}) - \varphi^{\dagger}(\mathbf{x})\left((\partial_\alpha + iA_\alpha)^2\varphi(\mathbf{x}) + \frac{1}{4}(\partial_\beta\hat{\mathbf{n}}\cdot\partial_\beta\hat{\mathbf{n}}) + J_{\mathrm{H}}\right)\varphi(\mathbf{x}) + \left(\psi^{\dagger}(\mathbf{x})\Delta_\alpha(\mathbf{x})\partial_\alpha\varphi(\mathbf{x}) + \frac{1}{2}\psi^{\dagger}(\mathbf{x})(\partial_\alpha\Delta_\alpha(\mathbf{x}))\varphi(\mathbf{x}) + \text{h.c.}\right) - J_{\mathrm{AF}}(\partial_\beta\hat{\mathbf{n}}\cdot\partial_\beta\hat{\mathbf{n}})\Bigg], \tag{2.5}$$

where $\psi(\mathbf{x})$ and $\varphi(\mathbf{x})$ are, respectively, the field (annihilation) operators describing locally aligned and antialigned electrons, $\mathbf{x}$ is the position vector, $\hat{\mathbf{n}}(\mathbf{x})$ is the unit vector along the background spin direction, and A and Δ are vector potentials originating from a Berry phase and are defined by

$$A_\alpha(\mathbf{x}) = \frac{1}{2}\cos\theta(\mathbf{x})\partial_\alpha\phi(\mathbf{x}), \tag{2.6a}$$

$$\Delta_\alpha(\mathbf{x}) = -\partial_\alpha\theta(\mathbf{x}) + i\sin\theta(\mathbf{x})\partial_\alpha\phi(\mathbf{x}). \tag{2.6b}$$

Note that $\Delta_\alpha^{*}\Delta_\alpha = \partial_\beta\hat{\mathbf{n}}\cdot\partial_\beta\hat{\mathbf{n}}$. Also note that in passing to the continuum limit we have retained only the lowest-order terms in the gradient expansion of the field operators. As a result, the electron kinetic energy, and hence the band structure that corresponds to it, is of a simple parabolic form.

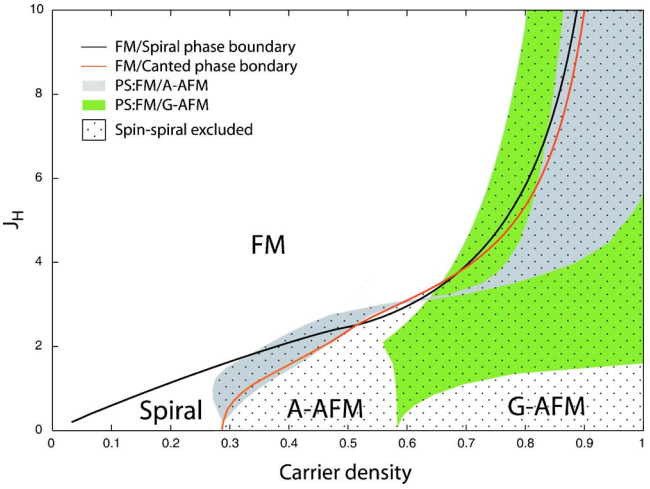

FIG. 4. (Color online) Dependence of the ground state of the double exchange model on the carrier density and the Hund coupling at zero antiferromagnetic coupling. At low carrier densities and high Hund couplings ferromagnetism is favored. In certain other regions, distinct homogeneous states are favored, including spin spiral (see Fig. 6), A- and G-type antiferromagnetism (see Fig. 3). In yet other regions several types of FM/AFM microphase-separated states are favored. As explained in the text, the boundaries indicated for microphase-separated states are in fact stability limits; the true boundaries must lie within these stability limits. Only in undotted region can one be certain that the spin-spiral state is the favored state.

A. Symmetries of the continuum Hamiltonian

1. Local gauge invariance

The mapping from a vector (representing a classical spin) in three-dimensional space to a spinor in $SU(2)$ is defined up to an angle $\chi(\mathbf{x})$, an overall phase factor, which is a $U(1)$ gauge freedom,[21] i.e., under the simultaneous transformations

$$\mathbf{A}(\mathbf{x}) \to \mathbf{A}(\mathbf{x}) + \nabla\chi(\mathbf{x}) \quad \mathbf{\Delta}(\mathbf{x}) \to e^{2i\chi(\mathbf{x})}\mathbf{\Delta}(\mathbf{x}),$$

$$\psi(\mathbf{x}) \to e^{i\chi(\mathbf{x})}\psi(\mathbf{x}), \quad \phi(\mathbf{x}) \to e^{-i\chi(\mathbf{x})}\phi(\mathbf{x}), \tag{2.7}$$

the Hamiltonian is invariant.

2. Global spin rotation invariance

The Hamiltonian is also invariant under rotation of all the background spins by a global angle. One can show that the effect of a global rotation is identical to a gauge transformation. For example, let us consider rotations about the x axis by a small angle ω. The unit vector $\hat{n}(\mathbf{x})$ transforms to $\hat{n}'(\mathbf{x})$ where $\theta'(\mathbf{x}) \approx \theta(\mathbf{x}) - \omega\sin\phi(\mathbf{x})$ and $\phi'(\mathbf{x}) \approx \phi(\mathbf{x}) - \omega\cot\theta(\mathbf{x})\cos\phi(\mathbf{x})$. Notice that the above transformation leaves $\partial_\beta\hat{n}\cdot\partial^\beta\hat{n}$ invariant, but the vectors $\mathbf{A}(\mathbf{x})$ and $\mathbf{\Delta}(\mathbf{x})$ transform, up to first order in ω, in the following manner:

$$A_\alpha \to A_\alpha - \frac{\omega}{2}\partial_\alpha\left(\frac{\cos\phi}{\sin\theta}\right), \tag{2.8a}$$

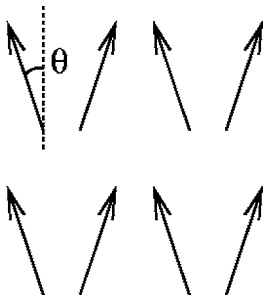

FIG. 5. Background spin configuration in the canted ferromagnetic state.

$$\Delta_\alpha \to \exp(-i\omega \cos\phi/\sin\theta)\Delta_\alpha. \tag{2.8b}$$

On identifying the factor $-\omega\cos\phi/2\sin\theta$ with the gauge parameter χ [see Eq. (2.7)], we see that Eq. (2.8a) describes a gauge transformation corresponding to rotations. A similar analysis can be carried out for rotations about the y axis; for rotations about the z axis the transformation is trivial. Therefore, global rotational invariance corresponds to the gauge freedom in the model.

B. Effective Hamiltonian

In this section we derive an effective Hamiltonian $H_{\rm eff}$ governing the spatially dependent background spin orientation (*texture*), in the limit that the texture varies on length scales much bigger than the inverse Fermi wave vector. To do this, we integrate out the electronic degrees of freedom, assuming that the zeroth-level description corresponds to a system in the presence of a spatially uniform texture. The contribution due to any inhomogeneity of the texture is then treated as a perturbation via a gradient expansion. The demerit of this continuum approach is that background spin configurations that change abruptly from one site to another (e.g., canted states or antiferromagnetic state) are excluded from consideration.

The effective Hamiltonian that results from this approach is a functional of $\mathbf{A}(\mathbf{x})$, $\mathbf{\Delta}(\mathbf{x})$, and $\hat{\mathbf{n}}(\mathbf{x})$ and their derivatives. Working at fixed chemical potential μ, the effective Hamiltonian is defined as

$$\begin{aligned}\exp(-\beta H_{\rm eff}[\mathbf{A},\mathbf{\Delta},\hat{\mathbf{n}},\mu]) &\equiv \int \mathcal{D}\psi\mathcal{D}\varphi \exp\{-\beta(H[\psi,\varphi,\mathbf{A},\mathbf{\Delta},\hat{\mathbf{n}}]-\mu N)\} \\ &= \int \mathcal{D}\psi\mathcal{D}\varphi \exp\{H_0[\psi,\varphi,\mu]+H_1[\psi,\varphi,\mathbf{A},\mathbf{\Delta},\hat{\mathbf{n}}]\},\end{aligned} \tag{2.9}$$

where $N\equiv\int d\mathbf{x}[\psi^\dagger(\mathbf{x})\psi(\mathbf{x})+\varphi^\dagger(\mathbf{x})\varphi(\mathbf{x})]$, H_0 is the free Fermi gas Hamiltonian, and the perturbation H_1 is a functional of $\mathbf{A}$, $\mathbf{\Delta}$, and $\partial\hat{\mathbf{n}}$, each of which has one spatial derivative [see Eq. (2.6a) and (2.6b)], and therefore is small in the sense of our approximation scheme. The form of $H_{\rm eff}$ is constrained by gauge invariance. Thus, keeping allowed terms to quartic order in gradients, but for now setting $J_{\rm AF}$ to zero, we find the following form, arranged in increasing order:

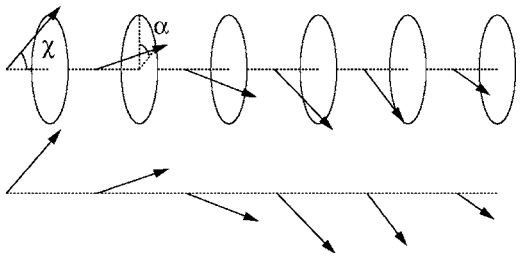

FIG. 6. Spin spiral configuration of background spins, with cone angle χ and wavevector α.

$$\begin{aligned}H_{\rm eff}[\mathbf{A}(x),\hat{\mathbf{n}}(x),\mathbf{\Delta}(x)] = \int d\mathbf{x}[&a(\mu)\partial_\alpha\hat{\mathbf{n}}\cdot\partial_\alpha\hat{\mathbf{n}} \\ &+ b(\mu)(\partial_\alpha\hat{\mathbf{n}}\cdot\partial_\alpha\hat{\mathbf{n}})^2 + c(\mu)F_{\alpha\beta}F_{\alpha\beta} \\ &+ d(\mu)|D_\alpha\Delta_\alpha|^2 + e(\mu)|D_\alpha\Delta_\beta|^2] \\ &+ \cdots,\end{aligned} \tag{2.10}$$

where the coefficients $a(\mu)$, $b(\mu)$, $c(\mu)$, $d(\mu)$, and $e(\mu)$ are evaluated by computing the corresponding Feynman diagrams. Not surprisingly, the results are compactly expressed in terms of the following quantities: $F_{\alpha\beta}\equiv\partial_\alpha A_\beta(x) - \partial_\beta A_\alpha(x)$ and $D_\alpha=\partial_\alpha-2iA_\alpha$; note that the combination $D_\alpha\Delta_\alpha$ is gauge invariant.

The Feynman diagrams contributing to the lowest-order terms in the gradient expansion are shown in Fig. 1. The amplitudes of these diagrams are both proportional to $(\partial^\alpha\hat{\mathbf{n}})^2$. Therefore, their coefficients, ρ_1 and ρ_2, add to give the stiffness of the ferromagnetic state ρ; when ρ goes negative, the ferromagnetic state becomes linearly unstable. The dependence of the corresponding limit of stability on d, μ, and $J_{\rm H}$ is among the central results of this paper. The contributions from these two diagrams compete with one another. The first gives a positive contribution to the energy, because a spatial variation of the background spins decreases the hopping amplitude, via the Anderson-Hasegawa mechanism: $t \to t\cos(\Theta_{ij}/2)$ where Θ_{ij} is the angle between the nearest-neighbor spins i and j in the discrete version of this model. The second diagram gives a negative contribution; spatial variations in the background spin orientation allow for mixing of aligned and anti-aligned bands, thereby lowering the energy. The contributions to the stiffness [i.e., the coefficient of $(\partial_\alpha\hat{\mathbf{n}})^2$] are

$$\rho_1 = \frac{(\mu+J_{\rm H})^{d/2}+(\mu-J_{\rm H})^{d/2}\Theta(\mu-J_{\rm H})}{2^{1+d}\pi^{d/2}d\,\Gamma(d/2)}, \tag{2.11a}$$

$$\rho_2 = \frac{(\mu+J_{\rm H})^{1+d/2}-(\mu-J_{\rm H})^{1+d/2}\Theta(\mu-J_{\rm H})}{2^{d+1}\pi^{d/2}(2+d)J_{\rm H}\Gamma(1+d/2)}, \tag{2.11b}$$

where $\Gamma[\cdot]$ is the gamma function, $\Theta[\cdot]$ is the Heaviside step function, and d is the dimension of space (see Appendix B).

By examining the stiffness as a function of μ and d (see Fig. 2) we observe that $d=2$ is a threshold dimension, in the sense that the instability occurs for dimensions less than two (but not for dimensions greater than two). We emphasize that

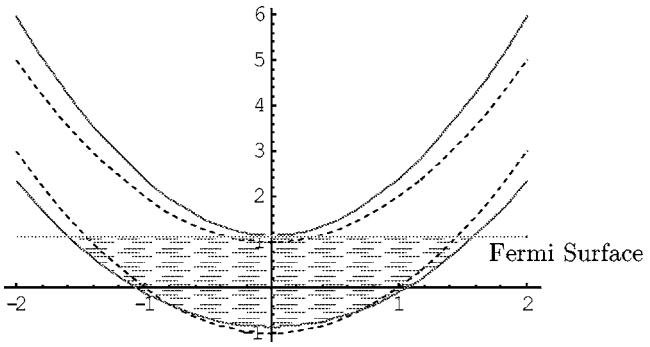

FIG. 7. Band structure in the presence (solid line) and absence (dashed line) of the spin-spiral magnetic state in two dimensions. Notice that the Fermi surface just touches the bottom of the antialigned band for the optimal spin-spiral state.

the precise location of the transition, as well as the threshold dimension, depends on the form of the bare electronic band structure, which we have taken to be parabolic. Corrections to the parabolic electronic dispersion relation would alter both the location of the transition and the threshold dimension.

In particular, in two dimensions the contributions combine to give the stiffness

$$\frac{J_{\mathrm{H}}^2-\mu^2}{32\pi J_{\mathrm{H}}}. \tag{2.12}$$

This shows that in two dimensions and at zero temperature there is a critical chemical potential $\mu_c=J_{\mathrm{H}}$ above which the ferromagnetic phase loses stability and, as we shall see, undergoes a transition to a "textured" phase. This critical chemical potential coincides with the bottom of the antialigned electron band. To investigate how the instability of the ferromagnetic state is resolved, it would therefore be necessary to raise the chemical potential above its critical value, which would begin populating this band. However, as the gradient expansion is an expansion powers of $q_{\mathrm{texture}}/k_{\mathrm{F}}^{\mathrm{upper}}$, it would not converge, as $k_{\mathrm{F}}^{\mathrm{upper}}$ would be very small. We approach this dilemma by noting that these results were obtained in the absence of an antiferromagnetic term in the original Hamiltonian 2.1, i.e., for $J_{\mathrm{AF}}=0$. The precise location $\mu_c(J_{\mathrm{H}},d)$ of the instability of the ferromagnetic state is perturbed, and in general shifted to lower value, in the presence of a positive J_{AF}, thus creating a region in the (μ,J_{AF}) plane in which the ferromagnetic state has become unstable and yet μ is still smaller than J_{AF}, so that the upper band remains unoccupied. This scheme opens up a region of the phase diagram in which our gradient expansion remains valid and, at the same time, a textured state is preferred.

In order to investigate the form of the (stable) textured state that replaces the (unstable) ferromagnetic state at chemical potentials immediately greater than the critical one (given in two dimensions by $\mu=J_{\mathrm{H}}$), we expand the effective Hamiltonian density to fourth order in gradients of $\hat{\mathbf{n}}$ and minimize it with respect to all textures that vary only on length scales longer than the Fermi wavelength. Via the extension to quartic order of the diagrammatic expansion described in the present section, and for the case of two dimensions, we find the effective Hamiltonian to be

$$\begin{aligned} H_{\mathrm{eff}} = & \frac{J_{\mathrm{H}}^2-\mu^2}{32\pi J_{\mathrm{H}}}(\partial_\alpha\hat{\mathbf{n}})^2+\frac{\mu(J_{\mathrm{H}}^2+\mu^2)}{256\pi J_{\mathrm{H}}^3}(\partial_\alpha\hat{\mathbf{n}})^4 \\ & +\frac{3J_{\mathrm{H}}^2(J_{\mathrm{H}}+\mu)-\mu^3}{48\pi J_{\mathrm{H}}^3}F^{\alpha\beta}F_{\alpha\beta} \\ & +\frac{(J_{\mathrm{H}}+\mu)^2(2J_{\mathrm{H}}-\mu)}{192\pi J_{\mathrm{H}}^3}|D_\alpha\Delta_\beta|^2-\frac{J_{\mathrm{H}}^3-\mu^3}{96\pi J_{\mathrm{H}}^3}|D_\alpha\Delta^\alpha|^2 \\ & -J_{\mathrm{AF}}(\partial_\alpha\hat{\mathbf{n}})^2, \end{aligned} \tag{2.13}$$

where the terms associated with J_{AF} arise from the antiferromagnetic term in Eq. (2.1).

The details of making this extension to quartic order are straightforward, and follow along the lines of Appendix B. For μ larger than its critical value, the coefficient of the first term in H_{eff} (e.g., the ferromagnetic stifness) is negative, and therefore it is favorable for the ground state to have a nonuniform texture. We now show that the remaining terms, which are fourth order in gradients and serve to restabilize the textured state, are all positive definite whenever $0<\mu<J_{\mathrm{H}}$. The coefficients of $(\partial_\alpha\hat{\mathbf{n}})^4$ and $F_{\alpha\beta}F_{\alpha\beta}$ are positive for $0<\mu<J_{\mathrm{H}}$, ensuring that these terms are indeed positive definite. If we neglect the surface terms, the forth and fifth terms can be recast in the following form:

$$\frac{\mu(J_{\mathrm{H}}^2-\mu^2)}{64\pi J_{\mathrm{H}}^3}|D_\alpha\Delta_\beta|^2+\frac{J_{\mathrm{H}}^3+\mu^3}{48\pi J_{\mathrm{H}}^3}\sin^2\theta\,|\nabla\theta\times\nabla\phi|^2. \tag{2.14}$$

In this form, the coefficients of each of these terms is positive for $0<\mu<J_{\mathrm{H}}$, and therefore all the fourth-order terms are indeed positive definite. Keeping only the first two terms, it is easy to check from the differential equation for the ground state, which follows from varying H_{eff} with respect to the fields θ and ϕ, that a spin spiral state (e.g., $\theta=\pi/2$ and $\phi=\mathbf{q}\cdot\mathbf{x}$, where $\mathbf{q}$ is a suitably chosen wave vector) minimizes the energy. The third, forth, and fifth terms vanish for the spiral state. Hence, the spiral state is a local minimum of the energy, as small perturbations around it would certainly increase the contribution from the first two terms, and the remaining terms can only give a positive contribution to the energy (as they are positive definite and zero to begin with). The implication of this analysis is as follows: in the double-exchange model there is a region of the zero-temperature (μ,J_{H}) phase diagram in which a spin spiral state is (at least locally) a stable ground state. This state emerges on the high-μ (or, equivalently, low-J_{H}) side of the continuous phase transition line, on the other side of which the ferromagnetic state is the stable state. By using the fourth-order terms to restabilize the instability caused by the negative stiffness and including the effects of J_{AF}, we find that the wave vector α of the spiral is given by

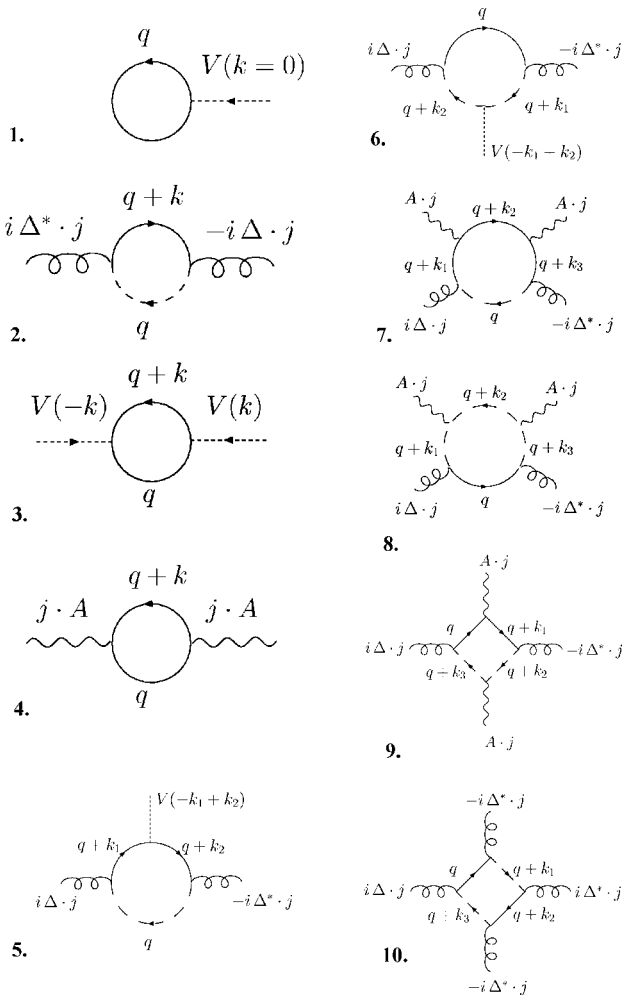

FIG. 8. Feynman diagrams associated with the Hamiltonian (2.5), contributing to the free energy up to fourth order in gradients of the background spin texture. Solid lines represent aligned electron propagators; dashed lines represent anti-aligned electron propagators; the remaining lines are labeled.

$$\alpha^2 = \frac{4J_H^2(\mu^2 - J_H^2 + 32\pi J_H J_{AF})}{\mu(\mu^2 + J_H^2)} \approx \frac{4(\mu - \mu_c)}{1 - 16\pi(J_{AF}/J_H)}, \tag{2.15}$$

where $\mu_c^2 = J_H^2(1 - 32\pi J_H J_{AF})$. The approximate form holds for $\mu \gtrsim \mu_c$.

Here, we note that if J_{AF} is greater than zero, then the spin-spiral would not persist to arbitrary small carrier density, as the antiferromagnetic state becomes stable. Is such a continuous transition preempted by a first-order transition into a microphase-separated state? We explore this possibility in the next section.

III. PHASE SEPARATED AND CANTED STATES

A. Collinear magnetic states

In this section we compare the energies of several commonly studied types of microphase-separated states[22] in double-exchange magnetic systems, with the aim of comparing their stability relative to the spin spiral state. By microphase separated we mean states that have mesoscale structure (magnetic and/or electronic) controlled by a competition between long-range interactions and interfacial energies. Prior work[9,20,22] has focused on the competition between the super-exchange and double-exchange coupling strengths, and has commonly assumed the latter to be infinite, or at least very large. In the present setting, we are concerned with the *entire* range of double-exchange coupling strengths, but only with small super-exchange coupling strengths.

In order to have the coexistence of the ferromagnetic and antiferromagnetic microphases associated with the microphase separation that we are considering, their thermodynamic and chemical potentials should coincide with one another.[19] These condition are necessary for microphase coexistence, but they are not sufficient in settings involving long-range interactions, such as those due to distinct charge-densities in the coexisting microphases, or interface energies associated with regions separating microphases. However, by examining the complement of the regions of the phase diagram that satisfy the aforementioned necessary conditions or are antiferromagnetic, we can locate the regions in which the homoegenous ferromagnetic state or the textured state have a chance of being stable. (As we shall be limiting our consideration to the various types of antiferromagnetic ordering listed in Fig. 3, we may fail to exclude some regions of the phase diagram that we shall be calling ferromagnetic or textured.)

We proceed by locating those regions of the (J_H, n) phase diagram in which either the conditions for microphase coexistance are satisfied or there is an antiferromagnetic state of lower energy than the ferromagnetic state. The single-electron band structure of the DE Hamiltonian (2.1) for ferromagnet (F), G-type (G), and A-type (A) antiferromagnet are given by

$$\text{(F)} \quad \epsilon_k = \pm J_H \pm 2t\cos k_x \pm 2t\cos k_y - \mu, \tag{3.1a}$$

$$\text{(G)} \quad \epsilon_k = \pm\sqrt{J_H^2 + 4t^2(\cos k_x \pm \cos k_y)^2} - \mu, \tag{3.1b}$$

$$\text{(A)} \quad \epsilon_k = \pm 2t\cos k_x \pm \sqrt{J_H^2 + 4t^2\cos^2 k_y} - \mu. \tag{3.1c}$$

For both antiferromagnetic arrangements (G and A), all the eigenvalues are doubly degenerate. The energy density and the electron density at zero temperature are given by

$$E = \int_{BZ} \frac{d^2k}{4\pi^2}\Theta(\epsilon_k)\epsilon_k, \tag{3.2a}$$

$$N = \int_{BZ} \frac{d^2k}{4\pi^2}\Theta(\epsilon_k), \tag{3.2b}$$

where for the antiferromagentic cases the Brillouin zone should be halved (in each direction), relative to the ferrmoagnetic case.

From these ingredients we find numerically the lines in the $(\mu, (J_H))$ plane at which the A-AFM/FM and G-AFM/FM phase transitions occur. On these phase boundaries, for each

pair of competing states we calculate a pair of lines $n_c(J_H)$ corresponding to the density of each state. On the (J_H,n) phase diagram these lines bound the regions depicted in Fig. 4 inside which the two competing microphases have a chance of coexisting.

B. Uniform canted magnetic states

Next we consider the instability of the ferromagnetic state with respect to the canted ferromagnet state, in order to determine the phase boundary between them. Repeating the proceedure of the previous subsection, we find the single-electron band structure of Eq. (2.1)

$$\epsilon_k = -2t\cos k_y - \mu \pm \sqrt{J_H^2 + 2t^2(1+\cos 2k_x) \pm 4J_H t \cos k_x \cos\theta}, \tag{3.3}$$

where θ is the canting angle of the background spin with respect to the z axis, as shown in Fig. 5. To find the phase transition line in the (μ,J_H) diagram, we determine when the stiffness of the ferromagnetic state with respect to canting becomes zero. The resulting phase-boundary line is shown in Fig. 4. From the diagram, it appears that the canted state is always preempted by a microphase-separated state.

IV. CONCLUDING REMARKS

To study smoothly varying textures of the double-exchange model, we have followed the familiar program of expanding the free energy of the model in powers of gradients of the background spin texture and tracing out the electronic degrees of freedom. This program has wide applicability to the study of long wavelength patterns in lattice models such as the double-exchange model. The main result of our paper is the phase diagram 4 for the double-exchange model, which we have obtained analytically as a function of the carrier density and the Hund coupling J_H between the carrier spins and the lattice of classical backgropund spins. Through the application of this program, we find that the spin-spiral state is indeed a stable state for low carrier-densities and has a continuously varying wave vector $\alpha \sim |\mu-\mu_c|^{1/2}$. By direct diagonalization we also find that the transition from the ferromagnetic state to the canted state is essentially preempted by phase separation into different types of antiferromagnetic states.

ACKNOWLEDGMENTS

We acknowledge helpful discussions with S. L. Cooper, D. I. Golosov, R. M. Martin, H. R. Krishnamurthy, T. V. Ramakrishnan, and M. B. Salamon. We are especially grateful to B. H. Lee for sharing with us his unpublished numerical work on the DEM, which prompted us to consider the issues addressed in the present paper. This work was supported by the U.S. Department of Energy, Division of Materials Sciences under Award No. DEFG02-91ER45439, through the Frederick Seitz Materials Research Laboratory, and the National Science Foundation under Grant No. DMR-9976550, and through the Materials Computation Center at the University of Illinois at Urbana-Champaign.

APPENDIX A: SIMPLE MODEL OF SPIN SPIRAL TEXTURE IN TWO DIMENSIONS

In this appendix, we solve for the exact ground-state energy of the DEM for the spin spiral state as the background spin texture. We confirm that in two dimensions the critical line for the transition lies at $\mu=J_H$, as stated in Sec. II B. The integrating-out of the electronic degrees of freedom, which we have carried out in the main text to determine the ground-state energy, becomes more transparent through this example, in which the process is nonperturbative. The simplification ensues when on restricts attention to a specific class of background spin configurations, viz., spin spirals, which have the form

$$\theta(x) = \chi; \quad \phi(x) = \alpha\cdot x, \tag{A1}$$

where α is a constant wave vector (Fig. 6). With this choice, $\mathbf{A}(x)=\alpha/2\cos\chi$, $\mathbf{\Delta}(x)=i\alpha\sin\chi$, and $(\partial_\mu\hat{\mathbf{n}})^2=\alpha^2\sin^2\chi$. The Hamiltonian (2.5) then reduces to

$$H_{2D} = \int (\psi^\dagger(k)\varphi^\dagger(k)) \begin{pmatrix} k^2+\alpha\cdot k\cos\chi+\alpha^2/4-J_H-\mu & -\alpha\cdot k\sin\chi \\ -\alpha\cdot k\sin\chi & k^2-\alpha\cdot k\cos\chi+\alpha^2/4+J_H-\mu \end{pmatrix} \begin{pmatrix} \psi(k) \\ \varphi(k) \end{pmatrix} \frac{d^2k}{4\pi^2}. \tag{A2}$$

On diagonalizing this Hamiltonian and calculating the effective energy for the spin spiral state, we find that the critical chemical potential is equal to the Hund coupling. The response of the band structure to the spin-spiral state is shown in Fig. 7. When μ is larger than J_H the ferromagnetic state is unstable with respect to the formation of a spin spiral state. For $\chi=\pi/2$ and $\mu<J_H$ the energy has the form

$$E_{\text{eff}} = -\frac{(J_H+\mu)^2}{8\pi} + \alpha^2\frac{J_H^2-\mu^2}{32\pi J_H} + \alpha^4\frac{\mu(J_H^2+\mu^2)}{256\pi J_H^3}. \tag{A3}$$

For $\mu>J_H$, minimizing E_{eff} with respect to α gives

$$\alpha^2 = \frac{4J_H^2(\mu^2-J_H^2)}{\mu(\mu^2+J_H^2)}, \tag{A4}$$

which determines the pitch of the stabilizing spin spiral.

APPENDIX B: EVALUATION OF FEYNMAN DIAGRAMS

In this appendix we present a sample diagram calculation by considering the two diagrams of lowest (i.e., second) order in the gradient expansion that determine the stiffness [i.e., $a(\mu)$ in Eq. (2.10); see Sec. II B]. We have computed the higher order diagrams in the same fashion, but specializing to two spatial dimentions.

The Matsubara Green functions for aligned (ψ) and antialigned (φ) electrons are

$$G_{\psi}(\mathbf{p},ip_n) = \frac{1}{ip_n - (p^2 - \mu - J_{\mathrm{H}})}, \tag{B1}$$

$$G_{\varphi}(\mathbf{p},ip_n) = \frac{1}{ip_n - (p^2 - \mu + J_{\mathrm{H}})}. \tag{B2}$$

The two diagrams that contribute to the ferromagnetic stiffness are diagrams 1 and 2 in Fig. 8. The amplitude corresponding to the first diagram is

$$\frac{1}{\beta}\sum_{iq_n} \int \bar{d}\mathbf{q}[G_{\psi}(\mathbf{q},iq_n) + G_{\varphi}(\mathbf{q},iq_n)]\frac{1}{4}(\partial_{\beta}\hat{\mathbf{n}} \cdot \partial_{\beta}\hat{\mathbf{n}}), \tag{B3}$$

where $\bar{d}\mathbf{q}$ stands for $d^dq/(2\pi)^d$. The integral over the internal momentum results in the following expression, which is essentially the the sum of the volumes of two d-dimensional spheres of respective radii $\sqrt{\mu - J_{\mathrm{H}}}$ and $\sqrt{\mu + J_{\mathrm{H}}}$:

$$\frac{2^{-1-d}\pi^{-d/2}\mu^{d/2}}{d\Gamma(d/2)}[\Theta(\mu + J_{\mathrm{H}})(\mu + J_{\mathrm{H}})^{d/2} + \Theta(\mu - J_{\mathrm{H}})(\mu - J_{\mathrm{H}})^{d/2}] \int d\mathbf{x}(\partial_{\beta}\hat{\mathbf{n}} \cdot \partial_{\beta}\hat{\mathbf{n}}). \tag{B4}$$

The amplitude corresponding to the second diagram is

$$\frac{1}{\beta}\sum_{iq_n} \int \bar{d}\mathbf{q}\bar{d}\mathbf{k} G_{\varphi}(\mathbf{q}+\mathbf{k},iq_n)G_{\psi}(\mathbf{q},iq_n) \times \Delta_{\mu}(\mathbf{k})\Delta^{*}_{\nu}(\mathbf{k})(q+k/2)_{\mu}(q+k/2)_{\nu} \tag{B5}$$

$$= \frac{1}{\beta}\sum_{iq_n} \int \bar{d}\mathbf{q}\bar{d}\mathbf{k} \times \frac{\Delta_{\mu}(\mathbf{k})\Delta^{*}_{\nu}(\mathbf{k})(q+k/2)_{\mu}(q+k/2)_{\nu}}{[iq_n - (q^2 - \mu - J_{\mathrm{H}})][iq_n - (|\mathbf{k}+\mathbf{q}|^2 - \mu + J_{\mathrm{H}})]}. \tag{B6}$$

On applying the standard Feynman trick and simplifying, the previous amplitude becomes

$$\frac{1}{\beta}\sum_{iq_n} \int \bar{d}\mathbf{q}\bar{d}\mathbf{k}\int_0^1 dz \frac{\Delta_{\mu}(\mathbf{k})\Delta^{*}_{\nu}(\mathbf{k})(q+k/2)_{\mu}(q+k/2)_{\nu}}{[(1-z)[iq_n - (q^2 - \mu - J_{\mathrm{H}})] + z(iq_n - (|\mathbf{k}+\mathbf{q}|^2 - \mu + J_{\mathrm{H}})\ ]^2} \tag{B7}$$

$$\approx \frac{1}{\beta}\sum_{iq_n} \int \bar{d}\mathbf{q}\bar{d}\mathbf{k}\int_0^1 dz \frac{\Delta_{\mu}(\mathbf{k})\Delta^{*}_{\nu}(\mathbf{k})q_{\mu}q_{\nu}}{[iq_n - q^2 + \mu - k^2 z + k^2 z^2 + J_{\mathrm{H}}(1-2z)]^2}, \tag{B8}$$

where in the final step we have dropped terms of higher order in $\mathbf{k}$, as they do not contribute to the stiffness. This follows from the obsevation that $\Delta^{*}_{\alpha}\Delta_{\alpha} = \partial_{\beta}\hat{\mathbf{n}} \cdot \partial^{\beta}\hat{\mathbf{n}}$. Reversing the order of summation and integration, and simplifying further by noting that the denominator sums to a δ function in the zero-temperature limit, we obtain

$$\int \bar{d}\mathbf{q}\bar{d}\mathbf{k}\int_0^1 dz \Delta_{\mu}(\mathbf{k})\Delta^{*}_{\nu}(\mathbf{k})(q_{\mu}q_{\nu})\delta[-q^2 + \mu - k^2 z + k^2 z^2 + J_{\mathrm{H}}(1-2z)] \tag{B9}$$

$$= \frac{-\Theta(\mu - J_{\mathrm{H}})(\mu - J_{\mathrm{H}})^{1+d/2} + \Theta(J_{\mathrm{H}} + \mu)(J_{\mathrm{H}} + \mu)^{1+d/2}}{2^{2+d}\pi^{d/2}J_{\mathrm{H}}\Gamma(2 + d/2)} \int d\mathbf{x}(\partial_{\beta}\hat{\mathbf{n}} \cdot \partial_{\beta}\hat{\mathbf{n}}), \tag{B10}$$

which simplifies to the expressions (2.11) in the text.

[1] T. V. Ramakrishnan, H. R. Krisdhnamurthy, S. R. Hassan, and G. Venkateswara Pai, cond-mat/0308396 (unpublished); S. Kumar and P. Majumdar, cond-mat/0406085 (unpublished).

[2] H. Ohno, A. Shen, F. Marsukara, A. Oiwa, A. Endo, S. Katsumo, and Y. Iye, Science **281**, 951 (1988); H. Ohno *et al.*, Appl. Phys. Lett. **69**, 363 (1996); T. Dietl, Semicond. Sci. Technol. **17**, 377 (2002); H. Akai, Phys. Rev. Lett. **81**, 3002 (1998).

[3] M. P. Kennett, M. Berciu, and R. N. Bhatt, Phys. Rev. B **66**, 045207 (2002).

[4] S. Kumar and P. Majumdar, Phys. Rev. Lett. **91**, 246602 (2003).

[5] C. Timm and A. H. MacDonald, Phys. Rev. B **71**, 155206 (2005).

[6] See the review by J. Konig, J. Schliemann, T. Jungwirth, and A. H. MacDonald, in Electronic Structure and Magnetism of Complex Materials, edited by J. D. Singh and D. A. Papaconstantopoulos (Springer, Berlin 2003); cond-mat/0111314 (unpublished); see also B. H. Lee, X. Cartoixa, N. Trivedi, and R. M.

Martin, cond-mat/0410051 (unpublished).

[7] C. Zener, Phys. Rev. **82**, 403 (1951); P. W. Anderson and H. Hasegawa, *ibid.* **100**, 675 (1955); P.-G. de Gennes, *ibid.* **118**, 141 (1960); see also D. P. Arovas and F. Guinea, Phys. Rev. B **58**, 9150 (1998).

[8] S. Yunoki, J. Hu, A. L. Malvezzi, A. Moreo, N. Furukawa, and E. Dagotto, Phys. Rev. Lett. **80**, 845 (1998); E. Dagotto, T. Hotta, and A. Moreo, Phys. Rep. **344**, 1 (2001).

[9] E. Dagotto, S. Yunoki, A. L. Malvezzi, A. Moreo, J. Hu, S. Capponi, D. Poilblanc, and N. Furukawa, Phys. Rev. B **58**, 6414 (1998).

[10] M. Hamada and H. Shimahara, Phys. Rev. B **51**, 3027 (1995); J. Inoue and S. Maekawa, Phys. Rev. Lett. **74**, 3407 (1995).

[11] L.-J. Zou, Q.-Q. Zheng, and H. Q. Lin, Phys. Rev. B **56**, 13669 (1997).

[12] M. Yu. Kagan, D. I. Khomskii, and M. V. Mostovoy, Eur. Phys. J. B **12**, 217 (1999).

[13] L. Sheng, H. Y. Teng, and C. S. Ting, Phys. Rev. B **58**, 8186 (1998).

[14] L. Yin, Phys. Rev. B **68**, 104433 (2003).

[15] A. Chattopadhyay, A. J. Millis, and S. Das Sarma, Phys. Rev. B **64**, 012416 (2001).

[16] E. Kogan, M. Auslender, and E. Dgani, cond-mat/0206018 (unpublished).

[17] D. J. Garcia, K. Hallberg, B. Alascio, and M. Avignon, Phys. Rev. Lett. **93**, 177204 (2004).

[18] P. M. Krstajic, V. A. Ivanov, F. M. Peeters, V. Fleurov, and K. Kikoin, Europhys. Lett. **61**, 235 (2003); P. M. Krstajic, F. M. Peeters, V. A. Ivanov, V. Fleurov, and K. Kikoin, Phys. Rev. B **70**, 195215 (2004).

[19] See, e.g., E. L. Nagaev, *Colossal Magnetoresistance and Phase Separation in Magnetic Semiconductors* (Imperial College Press, London, 2002).

[20] J. L. Alonso, J. A. Capitan, L. A. Fernandez, F. Guinea, and V. Martin-Mayor, Phys. Rev. B **64**, 054408 (2001).

[21] See, e.g., A. Auerbach, *Interacting Electrons and Quantum Magnetism* (Springer-Verlag, New York, 1998), p. 72.

[22] D. I. Golosov, J. Appl. Phys. **91**, 7508 (2002); H. Aliaga, B. Normand, K. Hallberg, M. Avignon, and B. Alascio, Phys. Rev. B **64**, 024422 (2001).

[23] In deriving the continuum limit we assume that the density of impurities is larger then the density of fermions. Thus, our approach only applies to DMS when the magnetic impurities are not very dilute. Coincidently, in this limit, the spin-orbit scattering is found to be negligible (Ref. 5).